PHYSICSAccess Research Paper
ISSN Online: 2756-3898, ISSN Print: 2714-500X https://doi.org/10.47514/phyaccess.2026.6.2.003

Crystallographic and Spectroscopic Analysis of Activated Carbon Derived from Microwave-Assisted KOH Activation of Banana Peels

Mary E Oni[1], John C Agomuo[2], Samuel M Udeh[2], and Salisu I Kunya[3]

[1] Department of Electrical/ Electronic Engineering, Faculty of Engineering and Technology, Nigerian Defence Academy, Kaduna, Kaduna State, Nigeria
[2] Department of Physics, Faculty of Science, Nigerian Defence Academy, Kaduna, Kaduna State, Nigeria
[3] Department of Applied Physics, Faculty of Science, Federal University of Technology, Babura, Jigawa State, Nigeria

Corresponding E-mail: maryoni@nda.edu.ng

Received 26-05-2026
Accepted for publication 29-06-2026
Published 10-07-2026

Abstract

KOH-activated carbon was prepared from banana peel waste by microwave heating (800 W) for 10, 20, 30, and 40 min with a constant KOH/precursor ratio of 1:1. The effect of irradiation time on crystal order and surface chemistry was systematically investigated by X-ray Diffraction (XRD) and Raman spectroscopy. XRD analysis showed that crystallinity and graphitization increased gradually with activation time; at 40 min, the crystallite size was 20.5 ± 0.6 nm and the microstrain was 0.00160. Raman spectroscopy showed a systematic evolution of the D/G band intensity ratio (ID/IG) from ~1.0 (carbonized) to a minimum of 0.75 at 30 min, indicative of optimised graphitic ordering. The 30-40 min samples showed the highest degree of graphitization, suggesting potential for enhanced electrical conductivity and charge-storage performance. These results demonstrate that microwave activation duration is a powerful parameter for tuning the structural properties of banana peel-derived activated carbon for energy and adsorption applications.

Keywords: Banana peel; activated carbon; microwave activation; XRD; Raman spectroscopy; graphitization; crystallinity; supercapacitor.

I. Introduction

Activated carbon (AC) is a highly porous carbonaceous material widely recognized for its exceptional adsorption capacity and versatile applications in environmental remediation, catalysis, and energy storage systems [1]. In electrochemical energy storage devices such as supercapacitors and batteries, the performance of activated carbon depends not only on its surface area and pore structure but also on its degree of graphitic ordering and crystallographic characteristics, which strongly influence electrical conductivity and charge transport [2–5]. Among the various biomass precursors investigated for activated carbon production, banana peels (Musa spp.) have attracted considerable attention because of their abundance, renewability, low cost, and high cellulose and hemicellulose contents, which provide an excellent carbon framework for the development of porous graphitic structures during thermal activation [6-7].

Potassium hydroxide (KOH) is one of the most effective

chemical activating agents for producing highly porous activated carbons. During activation, potassium species intercalate into carbon layers, promoting structural expansion, pore development, and partial graphitization of the carbon matrix [8]. When combined with microwave-assisted heating, KOH activation becomes significantly more efficient because microwave irradiation provides rapid volumetric heating and generates localized high-temperature regions ("hot spots") that accelerate carbonization, activation reactions, and structural ordering [9]. Consequently, microwave-assisted KOH activation can produce activated carbons with improved crystallinity and well-developed pore structures within considerably shorter processing times than conventional thermal activation methods [10].

The structural evolution of activated carbon during microwave activation is strongly dependent on irradiation time. X-ray diffraction (XRD) provides information on crystallite size, lattice parameters, and long-range crystallographic ordering, whereas Raman spectroscopy probes local structural disorder through the relative intensities of the graphitic (G) and defect-related (D) bands. Together, these complementary techniques provide a comprehensive understanding of graphitization and structural evolution in carbon materials [11-12]. Therefore, this study systematically investigates the influence of microwave activation time on the crystallographic and spectroscopic characteristics of banana peel-derived activated carbon using XRD and Raman spectroscopy.

II. Materials and Methods

A. Chemicals and Materials

Banana peels (Musa spp.) were obtained from local fruit vendors in Kaduna, Nigeria. The peels were thoroughly washed with distilled water, drained, cut into small pieces, and dried in a microwave oven at 400 W for 45 minutes to a constant weight. 200 g of dried banana peel was pyrolyzed in a limited oxygen atmosphere at 800 W for 2 hours to a final weight of 89.2 g. The pyrolyzed material was ground and sieved to below 250 µm. The reagents used are aqueous saturated KOH solution and HCl (both Sigma-Aldrich, Burlington, MA, USA), and distilled water.

B. Synthesis of Activated Carbons

Banana peel powder was mixed with saturated KOH solution at 1:1 by weight, stirred for 6 hours, then dried at 115°C. The KOH-impregnated precursor was activated at 800 W for 10, 20, 30, or 40 minutes under nitrogen. After cooling, the product was washed with 0.1 M HCl, rinsed to pH ≈ 7, and dried at 115°C for 12 hours. The resulting BPAC was stored in a desiccator for characterization.

C. Characterization

The crystalline structure of BPAC samples was analysed by X-ray Diffraction (XRD) using a PANalytical X'Pert PRO diffractometer (Cu Kα radiation, λ = 1.5406 Å, operating voltage 40 kV, current 40 mA). Patterns were recorded over 2θ = 10°- 80° at a step size of 0.02° and a scanning rate of 2°/min. Crystallite size (D) was determined from the most intense peak using the Scherrer equation given by (1). The Microstrain (ε) and crystallite size were evaluated simultaneously using the Williamson–Hall (W–H) plot given by (2), with regression performed by least-squares linear fitting ($R^2 = 0.94$). Miller indices (h k l) and d-spacings were calculated from observed peak positions using Bragg's law, with peak matching performed against the ICDD PDF-4+ database (JCPDS #01-049-1093). Monoclinic unit-cell parameters were refined from the indexed reflections.

$$D = \frac{K\lambda}{\beta \cos\theta} \quad (1)$$

where K = 0.9 (Scherrer constant), λ is the X-ray wavelength (1.5406 Å), β is the full width at half maximum (FWHM) in radians, and θ is the Bragg angle.

$$\beta \cos\theta = \left(\frac{K\lambda}{D}\right) + 4\varepsilon \sin\theta \quad (2)$$

A plot of β cos θ (y-axis) versus 4 sin θ (x-axis) yields a straight line; the y-intercept gives Kλ/D from which D is calculated, and the slope gives the microstrain ε.

The degree of graphitization and presence of structural defects were evaluated by Raman spectroscopy using a Horiba LabRAM HR Evolution spectrometer (532 nm diode laser excitation, laser power 1 mW at sample, 50× objective, spectral resolution 1 cm^{-1}, acquisition time 30 s, 3 accumulations). Spectra were recorded over 800-3200 cm^{-1}. Structural disorder was quantified by the intensity ratio of the D-band (~1350 cm^{-1}, disordered carbon) to the G-band (~1580 cm^{-1}, graphitic E_2g mode), denoted ID/IG. The second-order 2D (~2700 cm^{-1}) and D+G (~2900 cm^{-1}) combination features were also analysed.

III. Results and Discussion

A. X-ray Diffraction (XRD) Analysis

Fig. 1 shows the XRD patterns of carbonized banana peel and banana peel-derived activated carbon (BPAC) prepared by microwave-assisted KOH activation at 800 W for 10, 20, 30, and 40 min. The diffraction patterns reveal a progressive evolution in the crystalline structure of the activated carbon with increasing activation time. The carbonized precursor exhibits broad, low-intensity diffraction features characteristic of predominantly amorphous carbon. Following KOH activation, the diffraction peaks become progressively sharper and more intense, indicating improved crystallinity and graphitic ordering [13]. The 10 min sample remains largely amorphous, whereas the 20 min sample exhibits noticeable peak sharpening, suggesting the onset of structural ordering. More pronounced crystalline reflections emerge after 30 min of activation, while the 40 min sample displays the highest peak intensity and the narrowest diffraction features, indicating the greatest degree of long-range crystallographic order among the investigated samples.

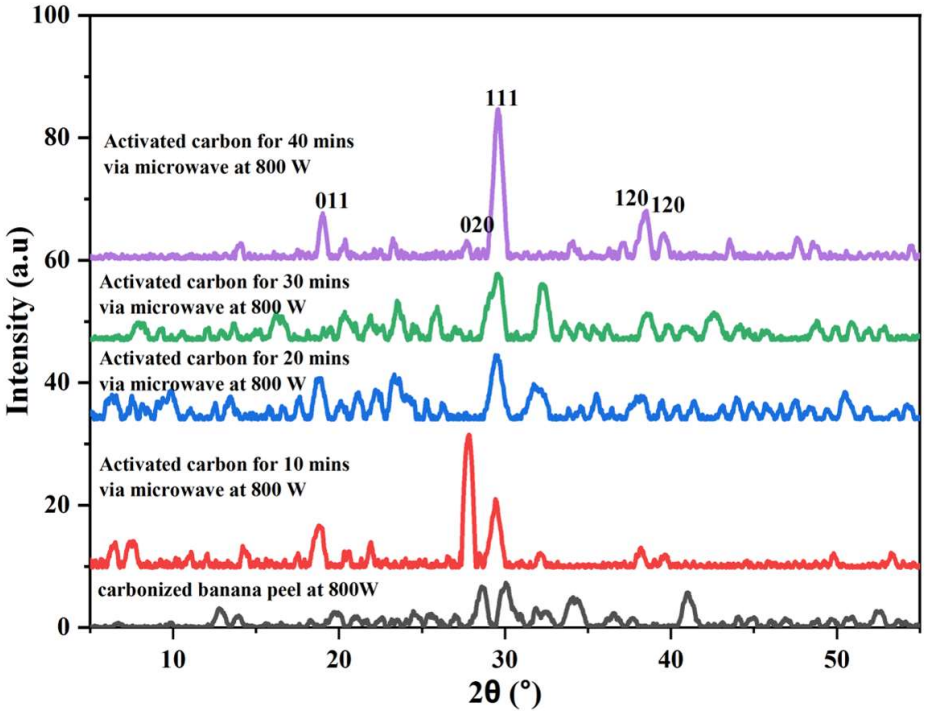

Fig. 1. XRD patterns for Carbonized Banana Peel and BPAC activated at 10, 20, 30, and 40 minutes at 800 W. Peak labels are indexed to a monoclinic K_2CO_3 phase (ICDD PDF #01-049-1093) and a turbostratic carbon phase.

To ensure accurate peak assignment, the reflections observed at approximately 29.57° and 29.91° (2θ), together with the associated (011), (020), (111), and (120) reflections, were indexed to the monoclinic K_2CO_3 phase (ICDD PDF No. 01-049-1093; space group $P2_1/c$; a = 3.73 Å, b = 6.04 Å, c = 7.25 Å, β = 86.8°), which forms from residual potassium species generated during KOH activation [14]. This assignment is consistent with the presence of non-zero off-axis reflections, whereas turbostratic carbon typically exhibits only broad (002) and (100) diffraction bands. In addition, the broad diffraction hump centred near 25–26.5° (2θ), corresponding to the turbostratic (002) stacking reflection, becomes progressively more intense with increasing activation time, confirming enhanced graphitic ordering alongside crystallization of the residual K_2CO_3 phase.

The observed structural evolution is consistent with the established activation mechanism of KOH. During microwave heating, KOH functions as both a dehydrating and activating agent, promoting the removal of oxygen- and hydrogen-containing functional groups while simultaneously generating extensive micro- and mesoporosity. These processes facilitate the rearrangement of carbon atoms into increasingly ordered graphitic domains, thereby improving the overall crystallinity of the activated carbon.

The crystallite size and lattice microstrain were evaluated using Williamson–Hall (W–H) analysis. As summarized in Table 1, the linear regression yielded an excellent correlation coefficient (R^2 = 0.94), confirming the reliability of the fitted model. The calculated average crystallite size of 20.5 ± 0.6 nm indicates the formation of relatively small but well-developed crystalline domains that are favourable for applications requiring high surface area and efficient ion transport [15]. The corresponding microstrain value of 0.00160 suggests minimal lattice distortion, implying improved structural stability and reduced charge-carrier scattering within the graphitic framework [15].

Table I. Williamson-Hall parameters and calculated crystallite size and microstrain for BPAC at 40 minutes. Linear regression R^2 = 0.94. Crystallite size uncertainty estimated from the standard error of the W-H y-intercept.

K	λ (Å)	Peak Position 2θ (°)	FWHM β (°)	x-axis $4\sin\theta$	y-axis $\beta\cos\theta$	Intercept $c = \frac{K\lambda}{D}$	Crystallite Size D (nm)	Micro-strain (ε)
0.9	1.5406	19.01	0.4079	0.6606	0.0070	0.0068	20.5 ± 0.6	0.00160
		29.57	0.5850	1.0206	0.0099			
		29.91	0.2547	1.0321	0.0043			
		38.41	0.6021	1.3159	0.0099			
		39.58	0.4333	1.3544	0.0071			

The indexed diffraction peaks and corresponding *d*-spacings are presented in Table II, while the refined monoclinic unit-cell parameters of the K_2CO_3 phase are listed in Table III. The refined lattice constants show excellent agreement with the ICDD reference data, providing further confidence in the crystallographic indexing and phase identification.

Table II. Miller indices (monoclinic K_2CO_3 phase, ICDD PDF #01-049-1093) and calculated d-spacings from Bragg's law.

Peak Position (2θ, °)	Miller Indices (h k l)	d-spacing (Å)
19.01	0 1 1	4.66
29.57	0 2 0	3.02
29.91	1 1 1	2.98
38.41	1 2 0	2.34
39.58	1 2 0	2.28

Table III. Refined monoclinic unit-cell lattice parameters for BPAC at 40 minutes.

A (Å)	b (Å)	c (Å)	B (°)	Unit Cell Volume (Å³)
3.73	6.04	7.25	86.8	162.5

The progressive increase in crystallinity with activation time has important implications for the potential electrochemical performance of BPAC. Improved structural ordering is generally associated with enhanced electron transport, more efficient ion diffusion pathways, and increased charge-storage capability. Similar trends have been reported for alkali-activated biomass-derived carbons, where increasing activation severity promotes graphitic ordering and consequently improves the physicochemical properties of the resulting activated carbon materials [16-17].

B. Raman Spectroscopy Analysis

Raman spectroscopy was employed to investigate the evolution of local structural ordering and defect density within the activated carbon framework. All spectra were recorded over the range of 800–3200 cm^{-1} and contain the characteristic first-order D (~1350 cm^{-1}) and G (~1580 cm^{-1}) bands together with the second-order 2D (~2700 cm^{-1}) and D+G (~2900 cm^{-1}) features. Variations in the ID/IG ratio provide valuable information regarding the balance between graphitic ordering and structural disorder during microwave activation.

1) Carbonized precursor

Fig. 2 shows the Raman spectrum of the carbonized precursor before KOH activation. Broad D and G bands of comparable intensity (ID/IG ≈ 1.0), together with the absence of a distinct 2D band, indicate a highly defective turbostratic carbon structure typical of biomass chars produced at relatively low graphitization temperatures [18]. The high density of structural defects reflects the presence of disordered sp^2 domains interrupted by oxygen-containing functional groups.

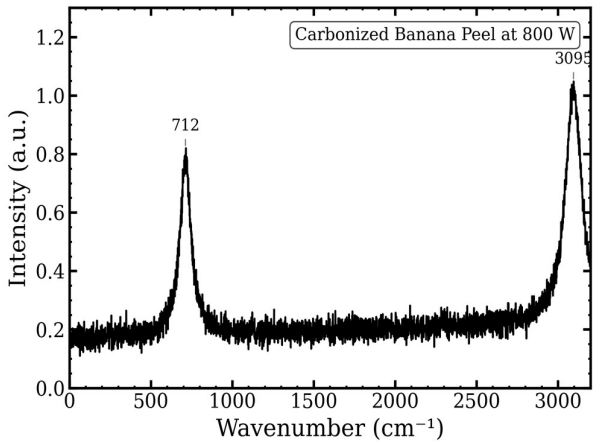

Fig. 2. Raman spectrum of (a) carbonized banana peel at 800 W (no KOH activation). Broad D and G peaks of near-equal intensity (ID/IG ≈ 1.0) and absence of a 2D band indicate a highly defective, amorphous turbostratic carbon structure.

2) 10 min activation

Following 10 min of microwave activation (Fig. 3), the D and G bands become slightly sharper, and a weak 2D shoulder emerges. Although the ID/IG ratio increases slightly (≈1.1–1.2), indicating that substantial disorder remains, the appearance of the 2D feature suggests that local graphitic domains have begun to develop. At this stage, microwave activation primarily removes volatile heteroatoms and initiates defect annealing while pore formation proceeds rapidly [19].

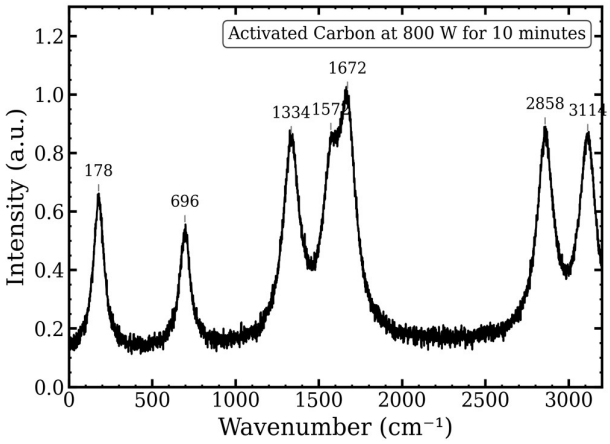

Fig. 3. Raman spectrum of (b) BPAC activated at 800 W for 10 minutes. Sharper D and G peaks (ID/IG ≈ 1.1-1.2) with a weak 2D shoulder suggest early-stage structural ordering, as significant disorder persists.

3) 20 min activation

The spectrum of the 20 min sample (Fig. 4) exhibits a marked reduction in the ID/IG ratio to approximately 0.9, together with a well-defined symmetric 2D band. These changes indicate increasing graphitic ordering and growth of sp^2 carbon domains. The reduction in structural disorder

suggests that carbon atom rearrangement increasingly dominates over defect generation during intermediate activation [20].

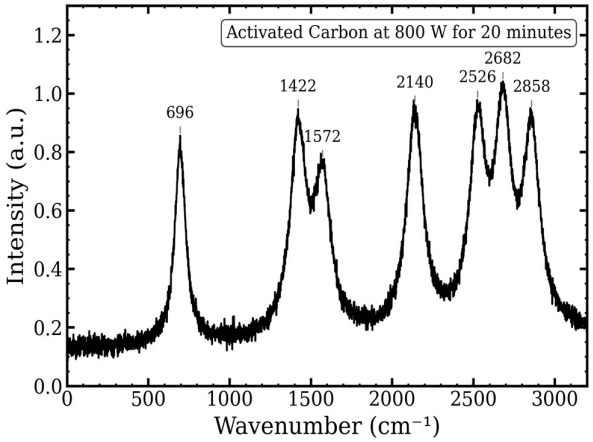

Fig. 4. Raman spectrum of (c) BPAC activated at 800 W for 20 minutes. ID/IG ≈ 0.9 with a distinct, symmetric 2D peak signals the onset of medium-range graphitic order.

4) 30 min activation

The greatest degree of local graphitic ordering is observed after 30 min of activation (Fig. 5), where the minimum ID/IG ratio (≈0.75), narrow G band, and strong 2D intensity collectively indicate the formation of large, coherent graphitic domains. This activation period appears to provide the optimum balance between defect healing and carbon removal, producing the highest local structural order within the series [11].

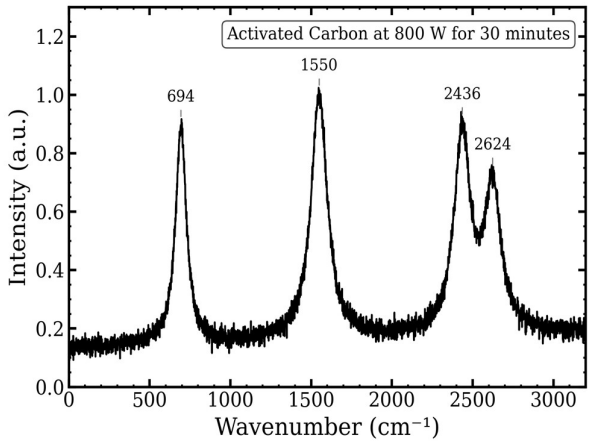

Fig. 5. Raman spectrum of (d) BPAC activated at 800 W for 30 minutes. ID/IG ≈ 0.75 with a narrow G band and strong 2D intensity indicates the largest, most coherent graphene domains, which is the optimal local graphitic ordering in this series.

5) 40 min activation

Prolonging the activation time to 40 min (Fig. 6) results in a slight increase in the ID/IG ratio to approximately 0.8 accompanied by broadening of the G band. These observations indicate that prolonged microwave exposure begins to generate new edge defects through over-etching of the carbon framework. Nevertheless, the relatively strong 2D feature demonstrates that the graphitic domains remain largely preserved despite the increase in local disorder [21-23].

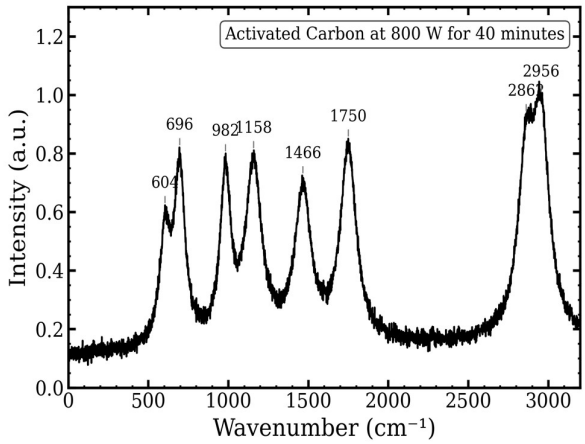

Fig. 6. Raman spectrum of (e) BPAC activated at 800 W for 40 minutes. ID/IG ≈ 0.8 with broadened G band indicates that over-etching introduces additional edge defects without fully degrading the graphitic domains.

Overall, the Raman results demonstrate that microwave activation initially promotes structural ordering through the elimination of oxygenated functional groups and progressive reorganization of carbon atoms into graphitic domains. Beyond the optimum activation time, however, continued activation preferentially erodes domain boundaries, producing additional edge defects without substantially disrupting the overall graphitic framework. Consequently, the 30 and 40 min samples are expected to exhibit superior electrical conductivity and charge-storage capability relative to the shorter activation times.

An important observation is the apparent difference between the XRD and Raman results. XRD identifies the highest degree of long-range crystallographic order in the 40 min sample, whereas Raman spectroscopy indicates that local graphitic ordering reaches its optimum after 30 min. These findings are complementary rather than contradictory because the two techniques probe different structural length scales. XRD measures long-range crystallographic coherence extending over multiple unit cells, whereas Raman spectroscopy is primarily sensitive to local bonding environments and edge defects at the nanometre scale. Consequently, prolonged activation can continue to improve long-range crystalline order while simultaneously generating additional edge defects that slightly increase the ID/IG ratio. This behaviour is consistent with the widely accepted two-stage graphitization mechanism in activated carbons, where crystallite growth and edge-defect evolution proceed semi-independently during extended thermal activation [11], [21-23].

IV. Conclusion

In this study, XRD and Raman spectroscopy were used to investigate the time-dependent structural and crystallographic evolution of banana peel-derived activated carbon (BPAC) prepared by KOH-induced microwave activation. The XRD analysis showed a clear trend of increasing crystallinity and graphitization with activation time, confirmed by the emergence of characteristic diffraction peaks for ordered carbon structures and K_2CO_3 (ICDD PDF #01-049-1093). Williamson-Hall analysis of the 40-minute sample yielded a crystallite size of 20.5 ± 0.6 nm and microstrain of 0.00160 (R^2 = 0.94). Raman spectroscopy revealed a systematic decrease in the ID/IG ratio from ~1.0 (carbonized) to a minimum of ~0.75 at 30 minutes, indicating optimum local graphitic ordering at this activation time. Prolonged activation to 40 minutes introduced additional edge defects at domain boundaries (ID/IG ≈ 0.80) while XRD continued to show improved long-range crystallographic order which is a distinction arising because XRD and Raman spectroscopy probe different length scales of structural organisation. The 30-40 min BPAC samples are expected to exhibit enhanced electrical conductivity and electrochemical performance for energy storage applications, providing a basis for future electrochemical validation.

Funding

This research received no external funding.

Conflict of Interest

The authors declare no conflicts of interest.

Reference

[1] H. Marsh and F. Rodríguez-Reinoso, Activated Carbon. Amsterdam, The Netherlands: Elsevier, 2006.

[2] K. Y. Foo and B. H. Hameed, "Microwave-assisted preparation and adsorption performance of activated carbon from biodiesel industrial solid residue," Chem. Eng. J., vol. 180, pp. 66–74, 2012.

[3] A. G. Pandolfo and A. F. Hollenkamp, 'Carbon Properties and their role in Supercapacitors,' J. Power Sources, vol.157, no. 1, pp. 11-27, 2006, doi: 10. 1016/j.jpower.2006.02.065.

[4] K. Yang, J. Peng, C. Srinivasakannan, L. Zhang, H. Xia, and X. Duan, "Preparation of high surface area activated carbon from coconut shells using microwave heating," Bioresour. Technol., vol. 101, no. 15, pp. 6163–6169, 2010, doi: 10.1016/j.biortech.2010.03.001.

[5] A. F. Hassan and A. M. Youssef, "A review on activated carbon: Essential aspects and microwave-assisted synthesis," J. Environ. Chem. Eng., vol. 8, no. 5, Art. no. 104143, 2020.

[6] N. A. Rashidi, S. Yusup, M. M. Ahmad, N. M. Mohamed, and B. H. Hameed, "Activated carbon from the renewable agricultural residues using single-step physical activation: A preliminary analysis," APCBEE Procedia, vol. 3, pp. 84–92, 2012, doi: 10.1016/j.apcbee.2012.06.051.

[7] P. González-García, "Activated carbon from lignocellulosic precursors by microwave-induced activation: A review," Ind. Crops Prod., vol. 112, pp. 691–703, 2018.

[8] M. A. Lillo-Ródenas, D. Cazorla-Amorós, and A. Linares-Solano, "Understanding chemical reactions between carbons and NaOH and KOH," Carbon, vol. 41, no. 2, pp. 267–275, 2003.

[9] J. A. Menéndez et al., "Microwave heating processes involving carbon materials," Fuel Process. Technol., vol. 91, no. 1, pp. 1–8, 2010.

[10] M. J. Ahmed and B. H. Hameed, "Microwave-assisted preparation of activated carbon from biomass: A review," J. Environ. Chem. Eng., vol. 7, no. 5, Art. no. 103262, 2019.

[11] H. Deng et al., "Preparation of activated carbons from cotton stalk by microwave-assisted KOH and K_2CO_3 activation," Chem. Eng. J., vol. 163, no. 3, pp. 373–381, 2010.

[12] P. L. Tang et al., "Characterization of activated carbon prepared from rice husks," Carbon, vol. 42, no. 11, pp. 2309–2312, 2004.

[13] Y. M. Xian et al., "Semi-quantitative analysis study of the impact of microwave treatment on fly ash," Physicochem. Probl. Miner. Process., vol. 59, no. 6, Art. no. 174897, 2023, doi: 10.37190/ppmp/174897.

[14] Y. Zhang et al., "In situ XRD/TGA of K_2CO_3 hydrate dehydration," J. Phys. Chem. C, vol. 127, no. 12, pp. 5892–5901, 2023.

[15] A. Abdisattar, M. Yerdauletov, M. Yeleuov, F. Napolskiy, A. Merkulov, A. Rudnykh, K. Nazarov, M. Kenessarin, A. Zhomartova, and V. Krivchenko, "The impact of biowaste composition and activated carbon structure on the electrochemical performance of supercapacitors," Molecules, vol. 29, no. 21, Art. no. 5029, 2024, doi: 10.3390/molecules29215029.

[16] I. Yanti, P. P. Sationo, W. F. Winata, M. Anugrahwati, A. K. Anas, and Y. A. Swasono, "Effectiveness of activated carbon magnetic composite from banana peel (Musa acuminata) for recovering iron metal ions," Case Stud. Chem. Environ. Eng., vol. 8, Art. no. 100378, 2023, doi: 10.1016/j.cscee.2023.100378.

[17] T. Mkilima, Y. Zharkenov, A. Abduova, N. Sarypbekova, N. Kudaibergenov, K. Sakanov, G. Zhukenova, Z. Omarov, P. Sultanbekova, and G. Kenzhaliyeva, "Utilization of banana peel-derived activated carbon for the removal of heavy metals from industrial wastewater," Case Stud. Chem. Environ. Eng., vol. 10, Art. no. 100791, 2024, doi: 10.1016/j.cscee.2024.100791.

[18] D. M. Keown, J.-I. Hayashi, C.-Z. Li, and T. Chiba, "Evolution of biomass char structure during oxidation in O_2 as revealed with FT-Raman spectroscopy," Fuel Process. Technol., vol. 89, no. 11, pp. 1259–1263, 2008.

[19] A. C. Ferrari and J. Robertson, "Resonant Raman spectroscopy of disordered, amorphous, and diamond-like carbon," Phys. Rev. B, vol. 64, Art. no. 075414, 2001.

[20] A. C. Ferrari and J. Robertson, "Interpretation of Raman spectra of disordered and amorphous carbon," Phys. Rev. B, vol. 61, no. 20, pp. 14095–14107, 2000.

[21] Li Li Zhang, Rui Zhou, X. S. Zhao; Graphene-based materials as supercapacitor electrodes. J. Mater. Chem. 2010; 20 (29): 5983–5992. https://doi.org/10.1039/c000417k.

[22] J. Chen, C. Li, and G. Shi, "Graphene Materials for Electrochemical Capacitors," J. Phys. Chem. Lett., vol. 4, no. 8, pp. 1244–1253, 2013, doi: 10.1021/jz400160k.

[23] Q. Ke and J. Wang, "Graphene-based materials for supercapacitor electrodes – A review," J. Materiomics, vol. 2, no. 1, pp. 37–54, 2016, doi: 10.1016/j.jmat.2016.01.001